Journal of Statistical Mechanics:
Theory and Experiment

PAPER: BIOLOGICAL MODELLING AND INFORMATION

Noise-induced transition in human reaction times

OPEN ACCESS

Journal of Statistical Mechanics: Theory and Experiment
An IOP and SISSA journal

ERRATUM

Erratum: Noise-induced transition in human reaction times (2016 *J. Stat. Mech.: Theory Exp.* 9 093502)

José M Medina and José A Díaz

Universidad de Granada, Facultad de Ciencias, Departamento de Óptica, Edificio Mecenas, 18071, Granada, Spain
E-mail: jmedinaru@cofis.es

Received 5 May 2020
Accepted for publication 8 June 2020
Published 6 August 2020

Online at stacks.iop.org/JSTAT/2020/089901
https://doi.org/10.1088/1742-5468/aba0a8

Due to an error, the two limiting regimes of the theory were interchanged. We regret to inform the readers that equation (16) in [1], that describes the ratio of the additive to the multiplicative noise in human reaction times, is flawed. Here, we report the correct expression, and, accordingly the modified figures 2(b), 3, and 4.

In section 3.1.2, the random multiplicative model of Piéron's law implies a chronological order that must be preserved. That is, the encoding time t_0 precedes the asymptotic term or plateau t_{RT_0}, and both precede the mean reaction time (RT), μ, $(0 < t_0 < t_{\mathrm{RT}_0} < \mu)$. The plateau t_{RT_0} is the irreducible part of Piéron's law and represents a repulsion barrier from the origin located at the encoding time, t_0, $(t_{\mathrm{RT}_0} = t_0 \ \exp(2 \ \ln \ 2\Delta H) > t_0, \forall \ \Delta H > 0)$. At supra-threshold conditions, the mean RT μ in Piéron's law always drifts to the plateau $(\forall \ I > I_0 \Rightarrow \mu \to t_{\mathrm{RT}_0})$, and thus, t_{RT_0} represents a bona fide additive noise term [2–4].

In page 8, the multiplicative, D_a, and additive diffusion coefficient, D'_b, should be written as follows:

$$D_a \cong \exp(2 \ \ln \ 2\Delta H) \left[\left(\frac{I_0}{I} \right)^p + \left(\frac{I_0}{I} \right)^{2p} + \cdots \right] \geqslant 0. \tag{1}$$

$$D'_b = \exp(2 \ \ln \ 2\Delta H) \geqslant 1, \tag{2}$$

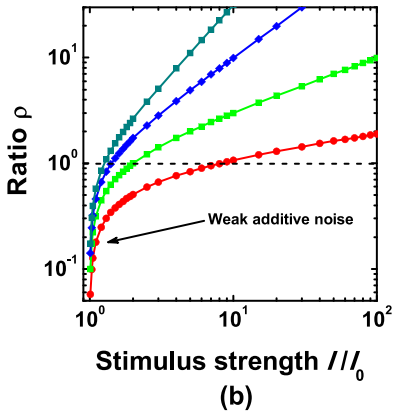

Figure 2. (b) Double logarithmic plot of the ratio ρ as a function of the normalized stimulus strength for different values of the exponent p. The horizontal black dashed line indicates a ratio equals to unity.

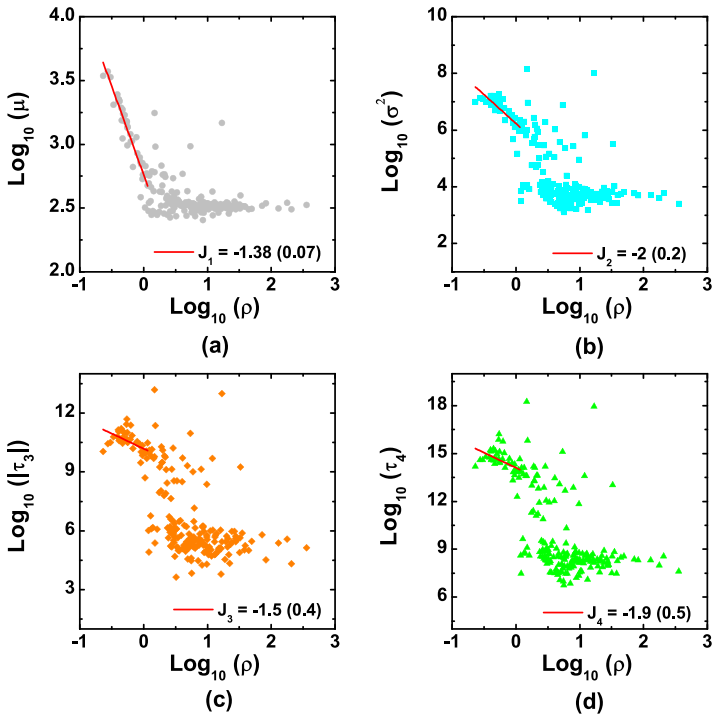

Figure 3. Double logarithmic plot ($\log_{10}$) of RT moments as a function of the ratio ρ for achromatic signals. (a) Mean value μ. (b) Variance σ^2. (c) Absolute value of the third-order moment $|\tau_3|$. (d) Fourth-order moment τ_4. In each panel, data points represent a total 216 of stimulus configurations. Red solid lines correspond to a linear regression analysis. The corresponding slopes are J_1, J_2, J_3, and J_4. Numbers in parentheses are ($\pm$ standard error).

Equations (1) and (2) replace equations (14b) and (15) in [1], respectively. Then, it follows in page 9, section 3.2, that the ratio ρ of the additive to the multiplicative noise

https://doi.org/10.1088/1742-5468/aba0a8

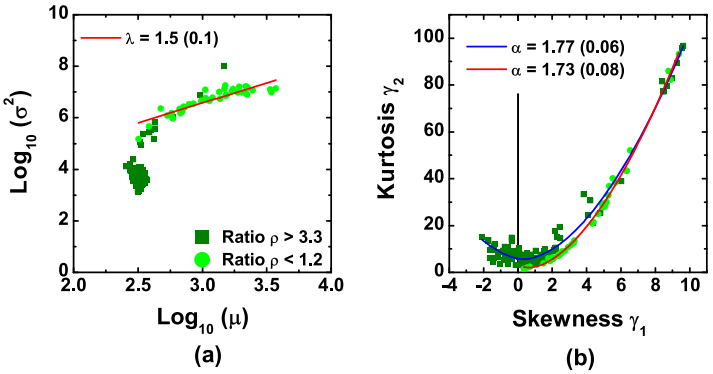

Figure 4. (a) Double logarithmic plot ($\log_{10}$) of the RT variance σ^2 as a function of μ for achromatic stimuli. Solid circles and squares indicate those RT stimulus configurations that correspond to a ratio $\rho < 1.2$ (weak additive noise), and $\rho > 3.3$ (strong additive noise), respectively. The red solid line corresponds to a linear regression analysis, $\log_{10}(\sigma^2) = \log_{10}(\eta) + \lambda \log_{10}(\mu)$, being η a coefficient, and λ the corresponding slope. (b) Linear plot of the kurtosis γ_2 as a function of the skewness γ_1 for the same RT data. Blue, and red solid lines indicate the best fit to the symmetric power function model with offset to those RTs in the strong ($\rho > 3.3$), and weak additive noise ($\rho < 1.2$), respectively, being α the scaling exponent in equation (2). In both panels, numbers in parentheses indicate (± standard error).

strength is written as:

$$\rho = \sqrt{\frac{D'_b}{D_a}} = \left[\sqrt{\left(\frac{I_0}{I}\right)^p + \left(\frac{I_0}{I}\right)^{2p} + \cdots}\right]^{-1} = \sqrt{\left(\frac{I}{I_0}\right)^p - 1}. \tag{3}$$

Therefore, equation (3) is the reciprocal of equation (16) in [1], and replaces it.

Here, the additive noise becomes small at near-threshold conditions, $\forall\, I \sim I_0 \Rightarrow \rho \to 0$; being stronger at marked supra-threshold conditions, $\forall\, I \gg I_0 \Rightarrow \rho \gg 1$. Therefore, when we said 'strong additive noise', it should be said, 'weak additive noise' and vice versa across the entire text in [1]. There is a noised-induced transition and the transition zone is now found at $\rho \approx 2$. Accordingly, the modified figures 2(b), 3 and 4 are provided below. The authors want to point out that these corrections do not affect the rest of analyses and discussion except the above cited changes. We apologize to the editor, and to the readers for any inconvenience caused.

References

[1] Medina J M and Díaz J A 2016 *J. Stat. Mech.: Theory Exp.* 093502
[2] Sornette D 1998 *Phys. Rev.* E **57** 4811–3
[3] Medina J M 2012 *Phys. Lett.* A **376** 1617–23
[4] Medina J M, Díaz J A and Norwich K H 2014 *Front. Hum. Neurosci.* **8** 1–4

Journal of Statistical Mechanics: Theory and Experiment
An IOP and SISSA journal

PAPER: Biological modelling and information

Noise-induced transition in human reaction times

José M Medina and José A Díaz

Departamento de Óptica, Universidad de Granada, Facultad de Ciencias, Edificio Mecenas, 18071, Granada, Spain
E-mail: jmedinaru@cofis.es

Received 21 June 2016, revised 24 August 2016
Accepted for publication 26 August 2016
Published 26 September 2016

Online at stacks.iop.org/JSTAT/2016/093502
doi:10.1088/1742-5468/2016/09/093502

Abstract. The human reaction/response time can be defined as the time elapsed from the onset of stimulus presentation until a response occurs in many sensory and cognitive processes. A reaction time model based on Piéron's law is investigated. The model shows a noise-induced transition in the moments of reaction time distributions due to the presence of strong additive noise. The model also demonstrates that reaction times do not follow fluctuation scaling between the mean and the variance but follow a generalized version between the skewness and the kurtosis. The results indicate that noise-induced transitions in the moments govern fluctuations in sensory–motor transformations and open an insight into the macroscopic effects of noise in human perception and action. The conditions that lead to extreme reaction times are discussed based on the transfer of information in neurons.

Keywords: fluctuation phenomena, information processing, noise models, pattern formation

1742-5468/16/093502+19$33.00

Contents

1. Introduction

The human reaction/response time (RT) has been a standard tool in the research on stochastic latency mechanisms in sensory and cognitive phenomena for more than a century [1–4]. RTs are common in everyday tasks and involve attention and rapid decision making at supra-threshold conditions. Typical examples can be found in sports performance (e.g. soccer players) [5], driving safety [6], chess [7], etc. At least three major types of experiment have reported the existence of two different regimes or phases in RTs. (i) The shape of the RT probability density function (pdf) is often right-skewed and depends on the external input signal. A transition is found as the stimulus strength I increases indicating the existence of a slow or 'sustained' and a fast or 'transient' temporal mechanism operating at low and high I values respectively [2, 8–14]. This sustained/transient transition is also an essential property of many sensory neurons [15] and has become an important approach for better understanding trial-to-trial RT variability and for modeling RT pdfs [2, 8, 12, 14]. (ii) Alternatively, the moments of RT pdfs also reflect the existence of a bi-phasic relationship. The mean RT μ (measured in milliseconds or ms) decreases as I increases [2, 17, 18] and shows a transition at high I values [19–21]. In vision research, the bi-phasic relation in the mean μ depends on the spatial frequency of gratings, adaptation level, retinal area and colourimetric properties of stimuli [19–26]. (iii) Fluctuation scaling relates trial-to-trial variability as measured by the sample variance σ^2 to the sample mean response approximately by a power function in many physical processes [27–30]:

J. Stat. Mech. (2016) 093502

$$\sigma^2 = \epsilon\mu^{\nu}, \tag{1}$$

ϵ and ν being the amplitude and the scaling exponent respectively [27–30]. The sample RT standard deviation σ or the variance σ^2 are correlated with the mean RT μ across stimulus conditions and they suffer deviations from fluctuation scaling by showing a bi-phasic relation. In general, there is an abrupt transition or knee and σ^2 saturates and reaches an asymptotic value for very large μ values [2, 12–14], [31–35].

Figure 1(a) shows an example of manual RTs in the (σ^2, μ)-plane for visual stimuli selected across the cardinal directions of the human colour space. The human colour space is an abstract three-dimensional representation of the colourimetric properties of visual stimuli. In colour coding, current models assert that L (long-), M (middle-) and S (short-) wavelength-sensitive cone photoreceptor signals are re-organized into three post-receptoral mechanisms or orthogonal cone axes: a luminance axis (L+M); and two chromatic-opponent cone axes at a constant luminance level or isoluminance: a red–green (L-M) axis and a blue–yellow axis [S-(L+M)]. Achromatic stimuli (i.e. black and white) stimulate the luminance system whereas red–green and blue–yellow stimuli at isoluminance stimulate the red–green and blue–yellow vision systems respectively [36], [37–40]. In figure 1(a), pattern formation in RTs shows a similar trend for both achromatic and isoluminant signals. The mean RT μ is often larger for isoluminance signals and the knee is observed for each visual signal separately [9, 36].

Together with the mean μ and the variance σ^2, the skewness γ_1 and the kurtosis γ_2 provide a quantitative description of heavy-tailed non-Gaussian RT distributions [31, 36]. RT pdfs are also correlated in the (γ_1, γ_2)-plane across stimulus conditions and follow a U-shaped pattern [36], in the same way as many variables in climate, plasma physics, finance, etc [30, 43–46]. Figure 1(b) shows the same experimental RT data in the (γ_1, γ_2)-plane. There is not an abrupt transition or knee and the U-shaped pattern is similar for achromatic and isoluminance stimuli. Pattern formation in the (γ_1, γ_2)-plane imposes important constraints for modeling RT pdfs [36]. The U-shaped pattern is quite sensitive to the existence of errors or extreme RT values from the tails of pdfs, specifically, false alarms and misses [36]. False alarms are anticipatory responses that produce very short RTs and left-skewed RT distributions ($\gamma_1 < 0$). Misses are rare RTs at the right tail of pdfs and produce very large kurtosis values ($\gamma_2 \gg 50$) [36]. A generalized version of fluctuation scaling has been proposed in the (γ_1, γ_2)-plane by using a symmetric power function model with offset [36, 47]:

$$\gamma_2 = \beta|\gamma_1 - S_{\mathrm{R}}|^{\alpha} + K_{\mathrm{R}}, \tag{2}$$

β, α, S_{R} and K_{R} being the amplitude, the scaling exponent, the center and the offset respectively. The parameters (S_{R}, K_{R}) indicate a lower bound that affects the overall location of data points. If $\gamma_1 \gg S_{\mathrm{R}}$ and $\gamma_2 \gg K_{\mathrm{R}}$, the symmetric power function model follows, $\gamma_2 \simeq \beta\gamma_1^{\alpha}$. In colour vision the scaling exponent is located between the asymptotic limit $\alpha = 4/3$ for very large γ_1 and γ_2 values [46, 47] and the quadratic function $\alpha = 2$ for moderate values [30, 43, 45], and is higher for achromatic ($\alpha \approx 1.8$) than isoluminant stimuli ($\alpha \approx 1.7$) [36].

In previous works, we have investigated the functional role of fluctuation scaling in human colour vision and visual masking at threshold. A random multiplicative model with weak additive noise explains pattern formation in the (σ^2, μ)-plane and in

J. Stat. Mech. (2016) 093502

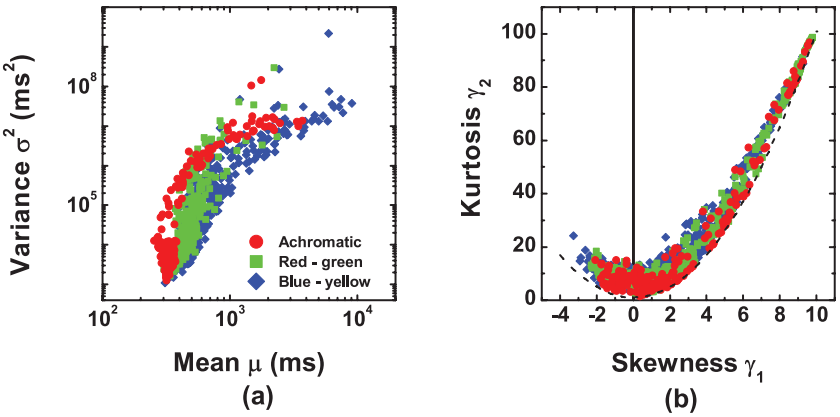

Figure 1. Statistical properties of RTs in human colour vision. (a) Double logarithmic plot ($\log_{10}$) of the variance σ^2 as a function of the mean μ for different visual stimuli selected across the cardinal directions of the colour space [36, 37, 40]. (b) Linear plot of the kurtosis γ_2 as a function of the skewness γ_1. The black dashed line indicates the statistical limit, $\gamma_2 = \gamma_1^2 + 1$ [41, 42]. The vertical solid line indicates the symmetric condition, $\gamma_1 = 0$. In both panels, each point corresponds to different stimulus configurations. The total number of experimental RTs was well over 126 000 and they were grouped in 1509 stimulus conditions [36].

the (γ_1, γ_2)-plane as well, with the additive noise term proportional to the contrast of mask stimuli [30]. We have also investigated fluctuation scaling at supra-threshold conditions by using RTs as exemplified in figure 1(b). Although pattern formation was similar in the (γ_1, γ_2)-plane at threshold and supra-threshold conditions [30, 36], it is not clear whether fluctuation scaling shares common generative mechanisms in both regimes. Deviations from fluctuation scaling in RTs as shown in figure 1(a) and reported elsewhere [2, 14, 31, 32, 34] suggest that fluctuation scaling could be the result of different processes in visual–motor communications at supra-threshold conditions. To elucidate these aspects, we will use an RT model based on Piéron's law. Piéron's law describes the hyperbolic decay of the mean RT μ as a function of stimulus strength I [1, 2, 17, 18], $\mu = t_{\mathrm{RT}_0} + \gamma I^{-p}$, t_{RT_0} being the asymptotic term or plateau reached at very high I values, and γ and p being coefficients, the latter controlling the hyperbolic decay [2, 17, 18, 31, 48, 49]. Piéron's law is valid in each sensory modality, in both simple and choice RTs and in certain animal models [2, 16, 18], [49–55]. In comparison with other approaches to RTs [2, 10], the RT model based on Piéron's law uses elements from statistical physics and information theory to define an universal efficient encoder in sensory communications [13, 48, 49, 51, 52]. In previous works, the RT model has provided a distinct mechanism that describes the bi-phasic relation type (i), i.e. the shape of RT pdfs as the result of a transition between log-normal and power-law pdfs [14]. We have also discussed the possible functional implications of sustained/transient mechanisms and power functions in RTs [4, 9, 16, 52, 56]. In this paper, we will investigate the RT model from a different perspective by examining the functional role of additive noise. We will provide a unifying description of bi-phasic relations type (ii) and type (iii), i.e. the bi-phasic behavior of the RT moments and departures from the power function of fluctuation scaling, equation (1), and the origin of equation (2) respectively.

J. Stat. Mech. (2016) 093502

Although noise is often considered a nuisance in neural systems, noise-induced phenomena can enhance the dynamics and stability properties in many bi-stable and threshold-based systems. Some examples are stochastic and coherence resonance, noise-induced synchronization, spatial patterns, etc [57–60]. Previous works have investigated the functional role of signal-dependent noise in sensory–motor communications [61–63] and fluctuation scaling in neurons [62, 64–67]. Here we report a different noise-induced process in mental chronometry. We demonstrate that bi-phasic relations type (ii) and type (iii) are mainly governed by a unique noise-induced transition in the moments of RT pdfs due to strong additive noise. The RT model also derives fluctuation scaling, equations (1) and (2), and explains pattern formation in the (σ^2, μ)-plane and in the (γ_1, γ_2)-plane in figures 1(a) and (b) respectively. We demonstrate that this noise-induced transition in the RT moments represents a non-trivial effect in sensory–motor communications and opens an insight into how noise-induced phenomena affect stochastic latency mechanisms in the brain at a macroscopic scale [30, 36, 59, 68].

The paper is organized as follows: in section 2, we describe the experimental methods and procedure used for RTs. We focus on RTs in human colour vision by using an extensive RT database that covers a wide range of stimulus conditions from different subjects [9, 14, 36, 69], [70]. In section 3 we derive the RT model based on Piéron's law. We discuss some of its basic properties by using a multiplicative growth process with additive noise and showing the existence of an internal threshold mechanism in RTs. Fluctuation scaling in equations (1) and (2) are derived from the RT model. We also present experimental results of a noise-induced transition in the mean RT μ. The RT model of Piéron's law generalizes the bi-phasic relationship in the mean μ type (ii) to higher-order moments and explains the bi-phasic relation type (iii). The implications in the temporal dynamics of parallel visual pathways and the origin of RT false alarms and misses are discussed in section 4. Conclusions are summarized in section 5.

2. Experimental methods

We have re-analyzed an RT database in colour vision containing more than 126 000 RTs from different subjects. The experimental methods and procedure are standard in visual psychophysics and colourimetry and have been reported elsewhere [9, 14], [36, 69–71]. Briefly, colour coordinates of visual stimuli were selected along the luminance direction and along the red–green and blue–yellow isoluminant directions of the human colour space. Stimuli were generated by using a colour calibrated display connected to a microcomputer equipped with a graphics card. At isoluminance, heterochromatic flicker photometry was used to match the luminance of red–green and blue–yellow stimuli to a reference adapting stimulus. RTs for chromatic variations at isoluminance were performed by using the hue-substitution method. The hue-substitution method avoids any luminance transient changes and RTs were measured for pure hue signals. All stimuli were uniform circular patches and were presented on a dark background. They were centered at the fovea in both monocular and binocular vision by using natural and artificial pupils. Subjects were seated in front of the colour display in a dark room. A chin rest was used for head stabilization. All subjects had normal

J. Stat. Mech. (2016) 093502

colour vision according with standard clinical tests and were experienced in RT tasks. For each subject, we collected a number of sessions across different days, months and years until reaching a distribution of no less than 70 RTs for each stimulus condition. For each session, subjects were allowed to adapt to darkness and to adapt to a reference stimulus. Different adapting stimuli were used at isoluminance. Subjects did not know which stimulus was the next in the sequence and their task consisted only of responding as soon as possible to an intensity change. RTs were measured for manual responses and were taken independently for each cardinal direction of the colour space. The computer clock was programmed to measure RTs with 1 ms accuracy.

3. Results

3.1. A human reaction time model

3.1.1. Piéron's law as a multiplicative process. Physics-based approaches to human RTs assert the existence of a cascade of random variables that control the time course of RTs in a certain chronological sequence or causal order [2, 3, 16, 49, 52, 53]. This formulation of RTs plays a central role to define not only an order but also a direction in the time axis. The time direction of RTs makes a parallelism with the definition of an irreversible process and can be characterized by an information entropy function as we will show below [48, 51, 72]. For a generic RT task, we define the growth of RT in the time axis at discrete steps to indicate the existence of different processes. The RT at the step $n+1$, x_{n+1}, depends on the previous step n, x_n, by means of a random multiplicative process with additive noise following a discrete-time Langevin equation [16, 52, 58, 73]:

$$x_{n+1} = a_n x_n + b_n + O(x_n^2) + \cdots, \tag{3}$$

a_n and b_n being the multiplicative and additive noise terms respectively. Equation (3) implies that x_n occurs before x_{n+1} and $0 < x_n \leqslant x_{n+1}$. When $a_n > 1$ and $0 < a_n < 1$, the magnitude of the RT is amplified or reduced respectively. The solutions of equation (3) are restricted within a lower and an upper bound. In the former, the additive noise term ($b_n > 0$) prevents x_{n+1} dropping to zero when a_n goes to zero and reaches a minimum RT value. In the latter, non-linear terms $O(x_n^2)$, etc keep the solution bounded up to a maximum RT value. Random multiplicative processes as in equation (3) are one of the simplest mechanisms that leads to power functions in such different fields as econophysics, noisy on–off intermittency in complex systems, etc [30, 58, 74–79]. Following the Langeving approach proposed by Nakao [79], it is established that $\langle a_n \rangle \propto D_a \neq 0$ and $\langle b_n \rangle \propto D_b \neq 0$, the brackets $\langle \cdots \rangle$ being the time average over many trials or repetitions of the same RT experiment. The factors D_a and D_b are the diffusion coefficients and indicate the average strength of interactions of the multiplicative and additive noise terms respectively. Applying the time average to equation (3) and considering only the first two terms on the right-hand side and $\langle a_n x_n \rangle \equiv \langle a_n \rangle x_0$, x_0 being a reference value related with an efficient encoder, the mean RT μ is the result of the interplay between the additive and multiplicative noise:

J. Stat. Mech. (2016) 093502

$$\mu \equiv \langle x_{n+1} \rangle \cong D_a x_0 + D_b. \tag{4}$$

It is assumed that both D_a and D_b are not fixed but elastic and that both are state-dependent and stimulus-driven. Equations (3) and (4) are an alternative way to rewrite Piéron's law, $\mu = t_{\mathrm{RT}_0} + \gamma I^{-p}$, by using a certain chronological sequence that cannot be violated [52, 53]. In equation (4), fluctuations in D_a and D_b across stimulus conditions are mapped into t_{RT_0}, γ and p.

3.1.2. A derivation of Piéron's law. To elucidate the internal structure of D_a and D_b as a function of t_{RT_0}, γ and p, we derive Piéron's law from first principles by using an informational theory proposed by Norwich [16, 48, 49, 51, 72]. In this framework, information processing in neurons is not instantaneous and always takes time. The RT can be defined as the time from stimulus presentation needed to gather ΔH bits of information [48, 51]:

$$\Delta H = H(I, t_0) - H(I, t) \geqslant 0. \tag{5}$$

The information entropy H is a Bolztmann-type entropy function that evolves continuously in time and provides a measure of the internal uncertainty state in sensory systems, t_0 and t being the encoding time and the time to react respectively. The encoding time t_0 in ΔH is an important variable and indicates the existence of a maximum entropy classifier or efficient encoder before reaction [49, 80]. The gain of information ΔH represents an irreversible process after efficient encoding and is linked with the formation of an internal variable threshold in the sensory system [16, 48, 49, 51–53]. In equation (5), a temporal sequence of events is implicit in the time axis and $0 < t_0 < t$. A plausible model for the information entropy function H can be written as follows [16, 48, 49, 51, 72]:

$$H = \frac{1}{2 \ln 2} \ln\left(1 + \frac{\phi I^p}{t}\right), \tag{6}$$

ϕ being a parameter. The information entropy as defined in equation (6) is a useful approach to examining the drop of internal uncertainty from a maximum entropy value or potential to receive information. Its origin is related to how sensory neurons transmit the information received by the sensory receptors about an external input signal of intensity I. The information entropy in equation (6) provides the basis to explain many empirical laws in human sensation and perception. Its mathematical derivation has been reported elsewhere [48, 51, 72]. Introducing equation (6) into equation (5):

$$\Delta H = \frac{1}{2 \ln 2} \left[\ln\left(1 + \frac{\phi I^p}{t_0}\right) - \ln\left(1 + \frac{\phi I^p}{t}\right) \right]. \tag{7}$$

Solving equation (7) for the time t [48, 51]:

$$t = \left[\frac{1}{t_0 \exp(2 \ln 2 \Delta H)} - \frac{1 - \exp(-2 \ln 2 \Delta H)}{\phi I^p} \right]^{-1}. \tag{8}$$

The asymptotic term or plateau in equation (8) is reached at very high stimulus strength [48, 51]:

$$\lim_{I\to\infty} t \equiv t_{\mathrm{RT}_0} = t_0 \exp(2\ln 2\Delta H). \tag{9}$$

The maximum value of t occurs for a just-threshold signal ($I = I_0$), I_0 being an internal threshold or reference value that depends on the stimulus configuration and ΔH [48, 49, 51]:

$$\lim_{I\to I_0} t \equiv t_{\mathrm{RT}_{\mathrm{MAX}}} = \left(\frac{1}{t_{\mathrm{RT}_0}} - \frac{1-\exp(-2\ln 2\Delta H)}{\phi I_0^p}\right)^{-1}. \tag{10}$$

Substituting the term $1-\exp(-2\ln 2\Delta H)$ from equation (10) into equation (8):

$$t = t_{\mathrm{RT}_0}\left[1-\left(1-\frac{t_{\mathrm{RT}_0}}{t_{\mathrm{RT}_{\mathrm{MAX}}}}\right)\left(\frac{I_0}{I}\right)^p\right]^{-1}. \tag{11}$$

Equations (8) and (11) show that RTs decay as a hyperbolic function of the stimulus strength I between an upper ($t_{\mathrm{RT}_{\mathrm{MAX}}}$) and a lower bound ($t_{\mathrm{RT}_0}$). If the difference between $t_{\mathrm{RT}_{\mathrm{MAX}}}$ and t_{RT_0} is large enough ($t_{\mathrm{RT}_0} \ll t_{\mathrm{RT}_{\mathrm{MAX}}}$), Piéron's law exists in RTs. In many practical situations, it is assumed that $t_{\mathrm{RT}_{\mathrm{MAX}}}$ is too large ($t_{\mathrm{RT}_{\mathrm{MAX}}} \to \infty$), i.e. lack of response at threshold. This issue will be discussed further later. Therefore, a generalized version of Piéron's law can be written as follows [16, 48, 49, 51]:

$$\mu \equiv\ t = t_{\mathrm{RT}_0}\left[1-\left(\frac{I_0}{I}\right)^p\right]^{-1}. \tag{12}$$

In equation (12), an RT response occurs only if ($I > I_0$). The classical form of Piéron's law [17] is obtained by taking the first two terms of the geometric series expansion in equation (12) [16]:

$$\mu = t_{\mathrm{RT}_0} + t_{\mathrm{RT}_0}\left[\left(\frac{I_0}{I}\right)^p + \left(\frac{I_0}{I}\right)^{2p} + \cdots\right], \tag{13}$$

and for the coefficient γ of Piéron's law, $\gamma \cong t_{\mathrm{RT}_0} I_0^p$ [16]. Here, $0 < t_0 < t_{\mathrm{RT}_0} < t$ [16, 49, 52, 53]. The multiplicative noise term in equation (4), $D_a x_0$, is related to the asymptotic term t_{RT_0} of Piéron's law [74, 77]:

$$x_0 = t_0 > 0, \tag{14a}$$

$$D_a = \exp(2\ln 2\Delta H) \geqslant 1. \tag{14b}$$

The diffusion coefficient of additive noise D_b in equation (4) also depends on the plateau t_{RT_0} but is mainly modulated by the reciprocal of the stimulus strength I. Taking the remaining terms of the geometric series expansion in equation (13), we rewrite $D_b = D_b' t_0$. D_b' can be expressed as follows:

$$D_b' \cong \exp(2\ln 2\Delta H)\left[\left(\frac{I_0}{I}\right)^p + \left(\frac{I_0}{I}\right)^{2p} + \cdots\right] \geqslant 0. \tag{15}$$

J. Stat. Mech. (2016) 093502

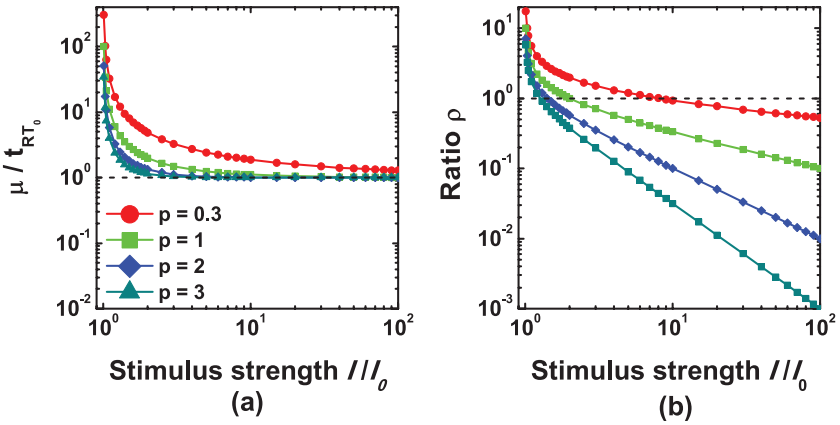

Figure 2. (a) Example of Piéron's law. Double logarithmic plot ($\log_{10}$) of the normalized mean RT (μ/t_{RT_0}) as a function of the normalized stimulus strength (I/I_0) for different values of the scaling exponent p. (b) Double logarithmic plot of the ratio ρ as a function of the normalized stimulus strength for different values of the exponent p. In both panels horizontal dashed black lines indicate a ratio equal to unity.

Figure 2(a) shows an example of Piéron's law by plotting the normalized mean RT (μ/t_{RT_0}) as a function of the normalized stimulus strength (I/I_0) for different values of the exponent p. The higher the value of p, the faster the hyperbolic decay [16, 48, 49, 51].

3.2. The effects of additive noise

To investigate power-law behavior of moments of RT pdfs, the Langevin approach made by Nakao compares the strength of the additive noise with respect to the multiplicative noise term under external driving [79]. The ratio ρ of the additive to the multiplicative noise strength can be defined as follows [79]:

$$\rho = \sqrt{\frac{D_b'}{D_a}} = \left[\sqrt{\left(\frac{I_0}{I}\right)^p + \left(\frac{I_0}{I}\right)^{2p} + \cdots}\right] = \left[\sqrt{\left(\frac{I}{I_0}\right)^p - 1}\right]^{-1}. \tag{16}$$

Figure 2(b) shows ρ as a function of the normalized stimulus strength (I/I_0) for different values of the exponent p. In general, ρ decreases as I increases and the scaling exponent p of Piéron's law controls the decay. The higher the value of p, the faster the decay ρ. The additive noise strength becomes small ($0 < \rho < 1$) at marked suprathreshold conditions ($I \gg I_0$). A balance is obtained when $\rho = 1$. However, strong additive noise effects ($\rho > 1$) are persistent in the critical region near the threshold ($I \cong I_0$). In this regime, the lower the value of the scaling exponent ($0 < p < 1$), the higher the additive noise strength (figure 2(b)).

When the effects of the additive noise strength are weak ($\rho \to 0$), Nakao [79] has demonstrated that the moments of the pdf in the Langevin model follow a power law as a function of ρ. The first moment is the mean μ and the second-order moment centered around the mean is the variance σ^2 [79]:

$$\mu \cong G_0 + G_1 \rho^{J_1}, \tag{17}$$

J. Stat. Mech. (2016) 093502

$$\sigma^2 \cong G_2 + G_3\rho^{J_2}, \tag{18}$$

G_0, G_1, G_2 and G_3 being coefficients and J_1 and J_2 the corresponding scaling exponents [30, 79]. To derive fluctuation scaling, we assume that $G_0 \cong 0$ and $G_2 \cong 0$ and introducing ρ from equation (17) into equation (18):

$$\sigma^2 = \left(\frac{G_3}{G_1^{\frac{J_2}{J_1}}}\right)\mu^{\frac{J_2}{J_1}}. \tag{19}$$

From this, and taking into account equation (1), the amplitude ϵ and the exponent ν of the standard version of fluctuation scaling are:

$$\epsilon = \frac{G_3}{G_1^{\frac{J_2}{J_1}}}, \tag{20a}$$

$$\nu = \frac{J_2}{J_1}. \tag{20b}$$

A similar treatment can be performed between the higher-order moments. Let τ_3 and τ_4 be the third- and fourth-order moments of the RT pdf, centered around the mean, respectively. Under the assumption of weak additive noise ($\rho \to 0$) [79]:

$$\tau_3 \cong G_4 + G_5\rho^{J_3}, \tag{21}$$

$$\tau_4 \cong G_6 + G_7\rho^{J_4}, \tag{22}$$

G_4, G_5, G_6 and G_7 being coefficients and J_3 and J_4 the corresponding exponents in the same way as in equations (17) and (18). Substituting ρ from equation (21) into equation (22):

$$\tau_4 = G_6 + \left(\frac{G_7}{G_5^{\frac{J_4}{J_3}}}\right)(\tau_3 - G_4)^{\frac{J_4}{J_3}}. \tag{23}$$

We assume that sensory systems are symmetric with respect to the offsets G_4, and G_6 in equations (21) and (22) [81]. The skewness γ_1 and the kurtosis γ_2 are the standardized third- and fourth-order moments respectively [82]: $\tau_3 = \gamma_1\sigma^{\frac{3}{2}}$, $\tau_4 = \gamma_2\sigma^2$. Therefore, the symmetric power function model in the (γ_1, γ_2)-plane becomes:

$$\gamma_2 = \left(\frac{G_6}{\sigma^2}\right) + \left(\frac{G_7\sigma^{\frac{3J_4}{2J_3}-2}}{G_5^{\frac{J_4}{J_3}}}\right)\left|\gamma_1 - \frac{G_4}{\sigma^{\frac{3}{2}}}\right|^{\frac{J_4}{J_3}}. \tag{24}$$

The amplitude β, the scaling exponent α and the offset (S_R, K_R) in equation (2) can be identified with the corresponding coefficients in equation (24):

J. Stat. Mech. (2016) 093502

$$\beta = \frac{G_7 \sigma^{\frac{3J_4}{2J_3}-2}}{G_5^{\frac{J_4}{J_3}}}, \tag{25a}$$

$$\alpha = \frac{J_4}{J_3}, \tag{25b}$$

$$S_{\mathrm{R}} = \frac{G_4}{\sigma^{\frac{3}{2}}}, \tag{25c}$$

$$K_{\mathrm{R}} = \frac{G_6}{\sigma^2}. \tag{25d}$$

3.3. Noise-induced transition

We investigate power-law behavior of equations (17), (18), (21) and (22) by using experimental RT data. The ratio ρ in equation (16) can be evaluated by providing an estimate of I_0 and p. In colour vision and contrast coding, the stimulus strength I is the contrast of stimuli. We have simplified the situation and have focused on RTs for achromatic visual signals. The RTs for red–green and blue–yellow signals at isoluminance follow in a similar way. For achromatic stimuli I can be defined as the standard Michelson contrast:

$$I = \frac{N_{\max} - N_{\min}}{N_{\max} + N_{\min}}, \tag{26}$$

$N_{\max}$ and $N_{\min}$ being the maximum and minimum luminance of stimuli with respect to the adapting reference stimulus [9, 14, 36]. Other contrast metrics [71, 83] produce similar results. The mean RT μ as a function of I was fitted to the generalized version of Piéron's law in equation (12) and the parameters I_0 and p were estimated. A weighted non-linear least-squares procedure was performed by minimizing the χ^2 statistics [84]. Weights were selected as the reciprocal of the RT standard deviation σ.

Figure 3 exemplifies in a double logarithmic plot the mean μ, the variance σ^2, the absolute value of the third-order moment $|\tau_3|$ and the fourth-order moment τ_4 of RTs as a function of the ratio ρ for achromatic signals. Although there are broadening effects [29], figure 3(a) clearly shows the existence of a noise-induced transition in the mean RT μ. This noise-induced transition represents the bi-phasic relationship type (ii) [20–23, 26], and is generalized to higher-order RT moments in figures 3(b)–(d). At supra-threshold conditions ($I \gg I_0$) the strength of additive noise is weak or transient ($\rho \to 0$) (see figure 2(b)). In figure 3, RT moments slightly increase as a function of ρ but the slopes are nearly flat and close to zero. A reliable estimation of the scaling exponents in equations (17), (18), (21) and (22) was not possible due to broadening [29]. However, at near-threshold conditions the additive noise is strong and produces a sustained behavior ($\rho \gg 0.8$) (see figure 2(b)). In this regime, RT moments in figure 3 increase as the ratio ρ increases and the slopes are higher than unity.

J. Stat. Mech. (2016) 093502

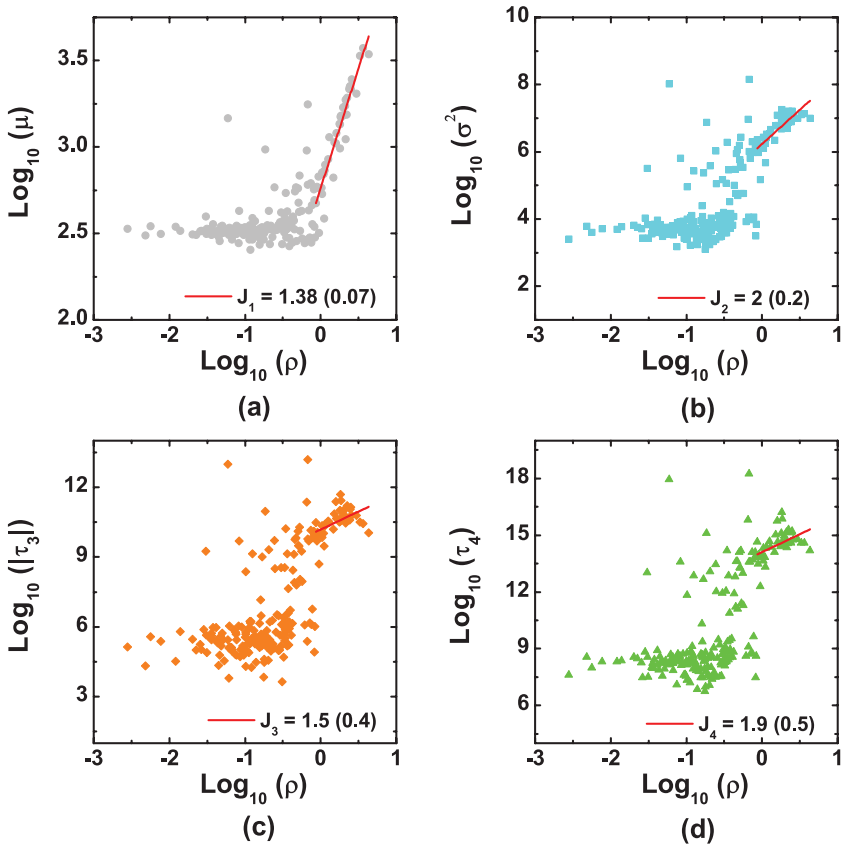

Figure 3. Double logarithmic plot ($\log_{10}$) of RT moments as a function of the ratio ρ for achromatic signals. (a) Mean value μ. (b) Variance σ^2. (c) Absolute value of the third-order moment $|\tau_3|$. (d) Fourth-order moment τ_4. In each panel, data points represent a total 216 of stimulus configurations. Red solid lines correspond to a linear regression analysis. The corresponding slopes are J_1, J_2, J_3, and J_4. Numbers in parentheses are (±standard error).

In all RT moments, there is a transition zone around $\rho \approx 0.5$ that separates the transient/sustained behavior. It is interesting to note that the transition zone is smoother for the mean RT μ (figure 3(a)) and becomes sharper for higher-order moments. Transition zones are similar between the variance, σ^2 and the third- $|\tau_3|$ and fourth-order τ_4 moments (figures 3(b)–(d)). These differences between transition zones explain the existence of a knee in the (σ^2, μ)-plane (figure 1(a)) and thus, the bi-phasic relation type (iii), whereas a similar knee in the (γ_1, γ_2)-plane is absent (figure 1(b)).

Figure 4(a) exemplifies in a double logarithmic plot the same RT data for achromatic signals in the (σ^2, μ)-plane. RTs at different stimulus conditions were classified into two groups: those σ^2 and μ values that correspond to weak additive noise ($\rho < 0.3$) and those that correspond to strong additive noise ($\rho > 0.8$). The remaining RT conditions around the transition zone ($\rho \approx 0.5$) were excluded. In figure 4(a) the two different regimes of the bi-phasic relation type (iii) are clearly discerned and avoid the existence of a single power function or the conventional version fluctuation scaling in equation (1) [28–30]. The transient or weak additive noise regime ($\rho < 0.3$) produces the lowest σ^2 and μ values. Figure 4(b) represents the same RT data in the (γ_1, γ_2)-plane. Those stimulus conditions for weak and strong additive noise lead to two different

J. Stat. Mech. (2016) 093502

U-shaped patterns. In the weak additive noise regime ($\rho < 0.3$), some RT distributions contain many false alarms and are left-skewed ($\gamma_1 < 0$). However, in the strong additive noise regime ($\rho > 0.8$) false alarms are minimized and RT distributions are right-skewed ($\gamma_1 > 0$).

The RT model with weak additive noise produces power-law behavior in the moments of pdfs as shown in equations (17), (18), (21) and (22) [79]. Power-law behavior of moments could also be extended to strong additive noise because Piéron's law is valid under both supra-threshold and near-threshold conditions (figure 2(a)). We investigate this issue in figure 3 in the strong additive noise regime ($\rho \gg 0.8$). A linear least-squared regression analysis for each RT moment was performed in a log–log plot. The scaling exponents for μ, σ^2, $|\tau_3|$ and τ_4 for strong additive noise were $J_1 = 1.38$, $J_2 = 2$, $J_3 = 1.5$ and $J_4 = 1.9$ respectively. In figure 4(a), a linear least-squared regression analysis was performed between σ^2 and μ in the strong additive noise regime and for the slope $\lambda = 1.5$. From equation (20*b*), the scaling exponent of fluctuation scaling ν leads to, $\nu \equiv (J_2/J_1) = 1.44$, which is a very good approximation to the slope λ. In figure 4(b), a non-linear least-squares procedure to the generalized version of fluctuation scaling, equation (2), was performed by minimizing the χ^2 statistics [84]. The scaling exponent α in the strong additive noise regime was $\alpha \approx 1.73$. From equation (25*a*), the scaling exponent of the symmetric power function model leads to $\alpha \equiv (J_4/J_3) = 1.26$, which is a reasonable approximation. It is interesting to note that the U-shaped pattern for achromatic signals found using raw RT data was $\alpha \approx 1.8$ [36]. This scaling exponent nearly matches the results obtained in the weak additive noise condition in figure 4(b) ($\alpha = 1.77$) [36]. However, raw RTs for both red–green and blue–yellow isoluminant signals show U-shaped patterns ($\alpha \approx 1.7$) that are closer to the strong additive noise condition in figure 4(b) ($\alpha \approx 1.73$) [36].

4. Discussion

4.1. Implications in neurophysiology

It has been argued that the bi-phasic relationship in the mean RT μ type (ii) for achromatic signals is mediated by different sub-cortical pathways [23, 25, 26], whereas the same bi-phasic relation is absent for chromatic signals at isoluminance [23–26]. We have extended previous works and generalized the bi-phasic relation type (ii) to higher-order RT moments, i.e. σ^2, τ_3 and τ_4 by using a RT database that contains a huge number of RTs spanning a broad range of stimulus conditions and several subjects [36]. The analyses of RT pdfs [9] and RT moments (figure 1) [36] are not compatible with a bi-phasic relation only for achromatic signals. The RT model based on Piéron's law demonstrates that bi-phasic relations type (ii) and deviations from fluctuation scaling or type (iii) are the result of a generic noise-induced transition due to strong additive noise. In both cases, a transient/sustained dynamics co-exist when using both achromatic and isoluminant stimuli (figures 1, 3 and 4).

Our approach is different from the random multiplicative model with weak additive noise used in visual masking at threshold [30]. First, the RT model derives Piéron's law which describes sensory–motor transformations by using a power

J. Stat. Mech. (2016) 093502

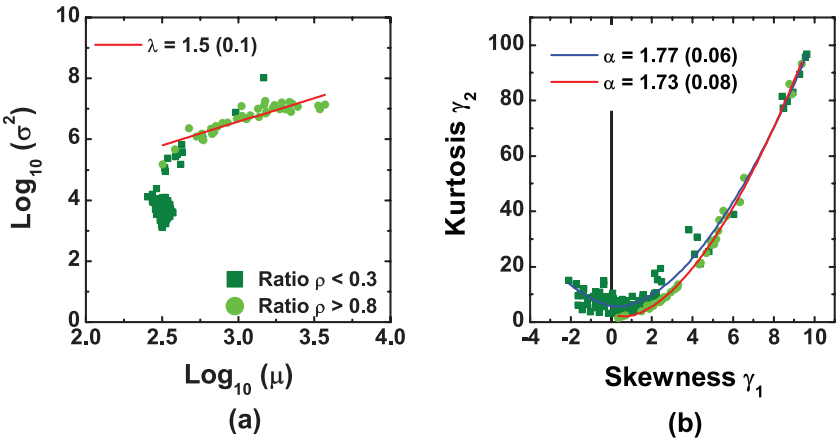

Figure 4. (a) Double logarithmic plot ($\log_{10}$) of the RT variance σ^2 as a function of μ for achromatic stimuli. Solid circles and squares indicate those RT stimulus configurations that correspond to ratios $\rho < 0.3$ (weak additive noise) and $\rho > 0.8$ (strong additive noise) respectively. The red solid line corresponds to a linear regression analysis, $\log_{10}(\sigma^2) = \log_{10}(\eta) + \lambda \log_{10}(\mu)$, η being a coefficient and λ the corresponding slope. (b) Linear plot of the kurtosis γ_2 as a function of the skewness γ_1 for the same RT data. Blue and red solid lines indicate the best fit to the symmetric power function model with offset to those RTs in the weak ($\rho < 0.3$) and strong additive noise ($\rho > 0.8$) respectively, α being the scaling exponent in equation (2). In both panels, numbers in parentheses indicate (±standard error).

function at supra-threshold conditions. Second, the ratio ρ in RTs as defined in equation (16), decreases as the stimulus strength I increases (figure 2(b)). However in visual masking, that ratio increases as the stimulus strength increases [30]. Third, the additive noise term of the RT model is not always weak as in visual masking [30, 79] but it becomes stronger at near-threshold conditions (figure 2(b)). Therefore, we conclude that there are distinct generative mechanisms that exhibit transient/sustained dynamics and modify fluctuation scaling in RTs at supra-threshold conditions. Differences between achromatic and isoluminant signals can be investigated by analyzing the scaling exponent α in the (γ_1, γ_2)-plane [30, 36]. Figure 4(b) demonstrates that both transient and sustained mechanisms produce U-shaped patterns with distinct α values. This is a crucial aspect that characterizes RTs for each visual signal. The results indicate that RTs for achromatic signals mainly contribute to the development of weak additive noise or transient dynamics ($\alpha \approx 1.8$) [36]. However, isoluminant signals often provoke strong additive noise or sustained dynamics in RTs ($\alpha \approx 1.7$) [36].

Piéron's law is invariant under transformations of scale in the time axis [14, 49, 85]. This property is similar to deflation or block renaming by means of a renormalization group approach in statistical physics. Self-similarity in Piéron's law at different time scales leads to an analogy with the reciprocal of the Naka–Rushton equation in neurophysiology [86]. The Naka–Rushton equation is considered a canonical form of gain control in neurons as a function of the stimulus strength [86–88]. Let $R = 1/t_{\mathrm{RT}}$ and $R' = 1/t_{\mathrm{RT}_0}$. Then, the Naka–Rushton equation can be derived from Piéron's law as follows [14, 49]:

J. Stat. Mech. (2016) 093502

$$R = \frac{R'}{1 + \left(\frac{I_0}{I}\right)^p}. \tag{27}$$

In equation (27), the neural response R (in spikes per second) increases as the stimulus strength I increases and then it saturates at high I values until reaching the asymptotic limit R'. The exponent of the Naka–Rushton equation p has the same role as in Piéron's law and controls the raise or the hyperbolic growth in equation (27). In RTs, p is related with microscopic neural interactions and different interpretations have been proposed [13, 14, 48, 49, 51, 89, 90]. In our case, gain control mechanisms as modeled by Piéron's law have a fundamental role and modulate the strength of the additive noise term under external stimulus driving (equation (16)). RTs for achromatic signals favour weak additive noise and, thus, their corresponding neural responses in equation (27) saturate sooner ($p_{\text{achromatic}} > 1$) [91, 92] (see also figure 2(b)). However, RTs for isoluminant signals promote strong additive noise. In accordance with equation (27), their associate neural responses are more linear and sustained and for the scaling exponent ($p_{\text{isoluminant}} < p_{\text{achromatic}}$) (figure 2(b)).

These RT differences between achromatic and isoluminant signals support the notion that noise-induced transitions in RT moments are mediated by the retinocortical magno-, parvo- and konio-cellular parallel pathways [39, 40, 93]. Magno cells combine L- and M-cone signals (L+M). They exhibit transient activity and respond better to achromatic stimuli. Their responses are faster and they saturate at high stimulus contrasts. However, parvo cells combine L-cones opposed to M-cones (L-M). They are more sustained and respond stronger to red–green stimuli at isoluminance. Their responses are slower and they do not saturate, and increase linearly as the stimulus contrast increases. Konio cells combine S-cones opposed to L- and M-cone signals [S-(L+M)]. They exhibit a sluggish delay in the visual cortex. They respond better to blue–yellow stimuli at isoluminance and their responses are heterogeneous at high stimulus contrasts [39, 40], [91–99].

4.2. Origin of false alarms and misses

The RT model based on Piéron's law governs the strength of the additive noise term (figure 2) if the difference between the lower t_{RT_0} and upper $t_{\text{RT}_{\text{MAX}}}$ bounds takes too large values (equation (11)). However, this is not always the case because the asymptotic term of Piéron's law, $t_{\text{RT}_0} = t_0 \exp(2 \ln 2 \Delta H)$ can be an unstable multiplicative process [76, 77], and the transfer of information ΔH acts as a bifurcation parameter when $\Delta H \to \infty$ [16].

Figure 5(a) exemplifies the effects of the upper and lower bounds in Piéron's law by taking different values of the ratio $(t_{\text{RT}_0}/t_{\text{RT}_{\text{MAX}}})$ in equation (11). In the limit $(t_{\text{RT}_0}/t_{\text{RT}_{\text{MAX}}}) \to 1$, Piéron's law almost disappears and becomes nearly flat near the threshold. From equation (10), the ratio $(t_{\text{RT}_0}/t_{\text{RT}_{\text{MAX}}})$ always decreases below unity as t_{RT_0} increases and guarantees the existence of Piéron's law in RTs. However, $(t_{\text{RT}_0}/t_{\text{RT}_{\text{MAX}}})$ also depends on the encoding time t_0 and the normalized threshold ϕI_0^p. The higher the value of ϕI_0^p in equation (10), the slower the decay will be and the ratio $(t_{\text{RT}_0}/t_{\text{RT}_{\text{MAX}}})$ will be closer to unity. This effect could prevent an efficient gain control of the additive noise strength in ρ (equation (16)) in certain situations.

J. Stat. Mech. (2016) 093502

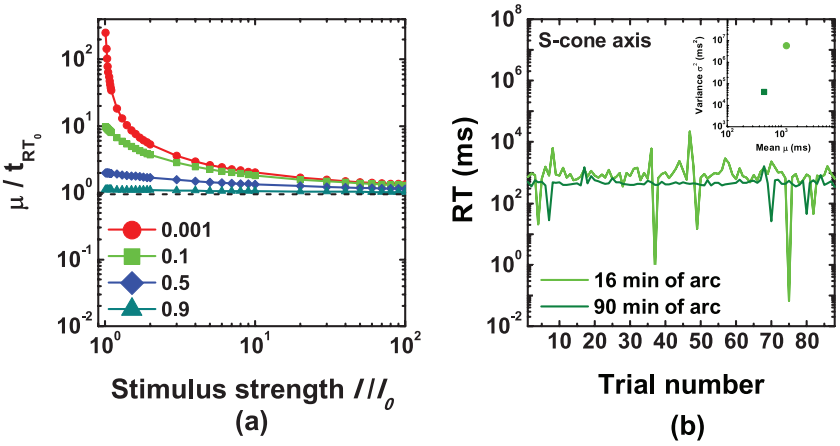

Figure 5. (a) The effects of boundary conditions on Piéron's law. Double logarithmic plot ($\log_{10}$) of the normalized mean RT (μ/t_{RT_0}) as a function of the normalized stimulus strength (I/I_0). Solid circles, squares, diamonds and triangles denote ratios ($t_{\mathrm{RT}_0}/t_{\mathrm{RT}_{\mathrm{MAX}}}$) of 0.001, 0.1, 0.5 and 0.9 respectively. (b) Semi-logarithmic plot of RT time series as a function of the trial number in the S-cone isolating axis. The example shows RTs for blue–yellow stimuli at isoluminance for two different stimulus sizes, 16 min or arc (S-cone free zone) and 90 min or arc. The inset shows, in a double logarithmic plot, the corresponding RT variance σ^2 as a function of the mean μ at 16 min or arc (circle) and 90 min or arc (square).

In general, the plateau t_{RT_0} is an auto-catalytic process where fluctuations in t_0 have a direct link with fluctuations in ΔH and vice versa. The multiplicative growth process indicates that t_{RT_0} decreases and $\Delta H \to 0$ as $t_0 \to \infty$. However, t_{RT_0} increases and $\Delta H \to \infty$ as $t_0 \to 0$ [76, 77]. We have investigated this issue by examining the effect of S-cone distribution in the human retina on RTs for blue–yellow changes at isoluminance. The spatial configuration of visual stimuli was 16 and 90 min of arc and they were centered at the fovea [70]. The former configuration allows us to stimulate the S-cone free zone in the central fovea or *foveola*. In the foveola, only L- and M-cone signals are available (usually called foveal tritanopia). However at 90 min of arc both L-, M- and S-cone signals are present [16, 70]. The paucity of S-cones at the foveola has a direct impact on RTs in the blue–yellow system [S-(L+M)]. The model of Piéron's law predicts that at 16 min of arc ΔH increases and t_0 decreases because only L- and M-cone signals are available in the blue–yellow channel and their corresponding latencies are shorter than S-cone signals [97]. Therefore, the plateau t_{RT_0} increases and by using Piéron's law and fluctuation scaling, the mean RT μ and the variance σ^2 are higher at 16 min of arc as demonstrated in figure 5(b). A similar result is obtained in the (γ_1, γ_2)-plane.

The asymptotic term t_{RT_0} is also state-dependent and varies between a minimum and a maximum value:

$$t_{\mathrm{RT}_{0\mathrm{MIN}}} = t_{0_{\mathrm{MAX}}} \exp(2 \ln 2 \Delta H_{\mathrm{MIN}}), \tag{28a}$$

$$t_{\mathrm{RT}_{0\mathrm{MAX}}} = t_{0_{\mathrm{MIN}}} \exp(2 \ln 2 \Delta H_{\mathrm{MAX}}). \tag{28b}$$

The minimum simple manual RT for visual signals is often considered to be between $t_{\mathrm{RT}_{0\mathrm{MIN}}} \cong 160$–$180$ ms [2, 100]. We conclude that optimal efficient encoding at $t_{0_{\mathrm{MAX}}}$ is

J. Stat. Mech. (2016) 093502

achieved when both L-, M- and S-cone signals are present. This is a manifestation of the principle of trichromacy in human colour vision [37–40] and involves different visual latencies across sub-cortical parallel pathways. This also implies that S-cone signals have a special role and modulates the plateau t_{RT_0} in the last instance because they exhibit larger latencies [96, 97]. In equation (28*a*) and after efficient encoding, the ratio of the two successive latencies ($t_{\mathrm{RT}_{0\mathrm{MIN}}}/t_{0_{\mathrm{MAX}}}$) asymptotically approaches the golden mean $\Phi = (1+\sqrt{5})/3 \equiv 1.618\,03\ldots$. The golden mean is a characteristic scaling factor and indicates how to subdivide the minimum length of the whole segment $t_{\mathrm{RT}_{0\mathrm{MIN}}}$ into the greatest common divisor $t_{0_{\mathrm{MAX}}}$ in the time axis. Consequently, the minimum transfer of information $\Delta H_{\mathrm{MIN}} \approx 0.347$ bits and for the optimal encoding time $t_{0_{\mathrm{MAX}}} \approx 98 - 111$ ms, which is a very good approximation to the sluggish response of S-cone signals in the primary visual cortex (96–135 ms) [96]. In equation (28*b*), magno cells (L+M) exhibit the shortest latencies at the visual cortex [97] and, $t_{0_{\mathrm{MIN}}} \approx 34$ ms [97]. We establish the maximum transfer of information as the value that leads to a stable geometric series expansion in equation (13), $\Delta H_{\mathrm{MAX}} \approx 4$ bits [16]. It follows that $t_{\mathrm{RT}_{0\mathrm{MAX}}} \approx 8700$ ms, i.e. nearly 55 times higher than $t_{\mathrm{RT}_{0\mathrm{MIN}}}$.

Those RTs outside the optimal range of efficient coding ($t_{0_{\mathrm{MIN}}}, t_{0_{\mathrm{MAX}}}$) can be considered as extreme values. Under this approach, false alarms are errors that result from bad coding ($t_0 \gg t_{0_{\mathrm{MAX}}}$) and promote a transfer of information in neurons below the minimum value allowed ($\Delta H < \Delta H_{\mathrm{MIN}}$). However, RT misses are errors that result from poor coding ($t_0 \ll t_{0_{\mathrm{MIN}}}$) and ($\Delta H > \Delta H_{\mathrm{MAX}}$). The results also indicate a counter-intuitive role for red–green and blue–yellow channels in temporal vision. It consists in exploiting the right amount of additive noise or the ratio ρ (equation (16)) to produce accurate visual–motor transformations within the efficient coding range. In colour vision, red–green and blue–yellow channels are considered second-order mechanisms with regard to their slower latencies [9, 69, 70, 94–97]. However, these chromatic-opponent channels can stabilize the temporal dynamics of the luminance system by promoting larger amounts of additive noise in such a way that the visual system stays in a sustained dynamics for a longer time. This could help to reduce false alarms in the analysis of complex visual scenes.

5. Conclusions

We have investigated the role of additive noise in a human RT model based on the information entropy H and Piéron's law, which is a universal feature for gain control at supra-threshold conditions. The model describes an irreversible process, $\Delta H \geqslant 0$, that is connected with the formation of an internal threshold in RTs. The RT model unifies bi-phasic relationships type (i) [16], (ii) and (iii); from RT pdfs [16], through the mean RT μ and higher-order moments, σ^2, τ_3 and τ_4, to deviations from fluctuation scaling in the (σ^2, μ)-plane and pattern formation in the (γ_1, γ_2)-plane. A noise-induced transition is revealed due to the presence of strong additive noise. This noise-induced transition provides a common basis for transient and sustained mechanisms in human colour vision. Our RT model can be also applied in the research into transient and sustained mechanisms in other sensory modalities such as in hearing, etc and abnormal sensory–motor transformations such as in Parkinson's disease, attention-deficit disorders, etc. The results open a

J. Stat. Mech. (2016) 093502

new perspective on the macroscopic effects of noise-induced phenomena, gain control and pattern formation in neurons in the (σ^2, μ)-plane [64, 65, 67] and in the (γ_1, γ_2)-plane [44] and may help to develop novel prostheses for sensory–motor impairments.

Acknowledgments

We thank Kenneth H Norwich (University of Toronto, Canada) for his help and support in the derivation of equations (10) and (11).

References

[1] Cattell J M 1886 *Brain* **8** 512–5
[2] Luce R D 1986 *Response Times* (New York: Oxford University Press)
[3] Meyer D E, Osman A M, Irwin D E and Yantis S 1988 *Biol. Psychol.* **26** 3–67
[4] Medina J M, Wong W, Díaz J A and Colonius H 2015 *Front. Hum. Neurosci.* **9** 1–3
[5] Montes-Mico R, Bueno I, Candel J and Pons A M 2000 *Optometry* **71** 775–80
[6] He Y, Rea M, Bierman A and Bullough J 1997 *J. Illum. Eng. Soc.* **26** 125–38
[7] Sigman M, Etchemendy P, Fernandez Slezak D and Cecchi G A 2010 *Front. Neurosci.* **4** 60
[8] Smith P L 1991 *Psychol. Rev.* **102** 567–93
[9] Medina J M and Díaz J A 2006 *J. Opt. Soc. Am.* A **23** 993–1007
[10] Smith P L and Ratcliff R 2004 *Trends Neurosci.* **27** 161–8
[11] Miller J and Ulrich R 2003 *Cognitive Psychol.* **46** 101–51
[12] Holden J G, Van Orden G C and Turvey M T 2009 *Psychol. Rev.* **116** 318–42
[13] Medina J M and Díaz J A 2011 *Applications of Optics and Photonics* (*Proc. SPIE* vol 8001) ed M F M Costa (Bellingham, WA: SPIE) pp 800131–9
[14] Medina J M and Díaz J A 2012 *J. Opt. Soc. Am.* A **29** A82–95
[15] Cleland B G, Dubin M W and Levick W R 1971 *J. Physiol.* **217** 473–96
[16] Medina J M 2012 *Phys. Lett.* A **376** 1617–23
[17] Piéron H 1914 *Ann. Psychol.* **20** 17–96
[18] Piéron H 1952 *The Sensations* (New Haven, CT: Yale University Press)
[19] Levi D M, Harwerth R S and Manny R E 1979 *Investigative Ophthalmol. Vis. Sci.* **18** 714–25
[20] Harwerth R S and Levi D M 1978 *Vis. Res.* **18** 1579–86
[21] Harwerth R S, Smith E L III and Levi D M 1980 *Perception Psychophys.* **27** 43–50
[22] Harwerth R S, Boltz R L and Smith E L III 1980 *Vis. Res.* **20** 15–22
[23] Plainis S and Murray I J 2000 *Neuropsychologia* **38** 1555–64
[24] Parry N R A 2001 *Color Res. Appl.* **26** S161–4
[25] Murray I J and Plainis S 2003 *Vis. Res.* **43** 2707–19
[26] Plainis S and Murray I J 2005 *Perception* **34** 933–40
[27] Taylor L 1961 *Nature* **189** 732–5
[28] Kendal W S 2004 *Ecol. Complex.* **1** 193–209
[29] Eisler Z, Bartos I and Kertsz J 2008 *Adv. Phys.* **57** 89–142
[30] Medina J M and Díaz J A 2016 *Phys. Rev.* E **93** 052403
[31] Baird J 1997 *Sensation and Judgement* (Mahwah, NJ: Lawrence Erlbaum Associates)
[32] Wagenmakers E J, Farrell S and Ratcliff R 2004 *Psychon. Bull. Rev.* **11** 579–615
[33] Iwaizumi A, Futami R, Kanoh S and Gyoba J 2006 *Biol. Cybern.* **94** 381–92
[34] Schmiedek F, Lvdn M and Lindenberger U 2009 *Psychol. Aging* **24** 841–57
[35] Servant M, Montagnini A and Burle B 2014 *Cogn. Psychol.* **72** 162–95
[36] Medina J M and Díaz J A 2016 *Physica* A **416** 125–32
[37] Wyszecki G and Stiles W S 1982 *Color Science* 2nd edn (New York: Wiley)
[38] De Valois R L, De Valois K K and Mahon L E 2000 *Proc. Natl Acad. Sci. USA* **97** 512–7
[39] Dacey D M 2000 *Ann. Rev. Neurosci.* **23** 743–75
[40] Solomon S G and Lennie P 2007 *Nat. Rev. Neurosci.* **8** 276–86
[41] Pearson K 1916 *Phil. Trans. R. Soc.* A **216** 429–57
[42] Wilkins J E 1944 *Ann. Math. Stat.* **15** 333–5
[43] Labit B *et al* 2007 *Phys. Rev. Lett.* **98** 255002

J. Stat. Mech. (2016) 093502

[44] Ringach D L and Malone B J 2007 *J. Neurosci.* **27** 7673–83
[45] Sura P 2011 *Atmos. Res.* **101** 1–21
[46] Cristelli M, Zaccaria A and Pietronero L 2012 *Phys. Rev.* E **85** 066108
[47] Giometto A, Formentin M, Rinaldo A, Cohen J E and Maritan A 2015 *Proc. Natl Acad. Sci.* **112** 7755–60
[48] Norwich K H 1993 *Information, Sensation, and Perception* (San Diego, CA: Academic)
[49] Medina J M 2009 *Phys. Rev.* E **79** 011902
[50] Pins D and Bonnet C 1996 *Perception Psychophys.* **58** 390–400
[51] Norwich K H, Seburn C N L and Axelrad E 1989 *Bull. Math. Biol.* **51** 347–58
[52] Medina J M, Díaz J A and Norwich K H 2014 *Front. Hum. Neurosci.* **8** 1–4
[53] Medina J M and Díaz J A 2015 *Front. Physiol.* **6** 1–4
[54] Wensveen P J, Huijser L A E, Hoek L and Kastelein R A 2014 *J. Exp. Biol.* **217** 359–69
[55] Mulsow J, Schlundt C E, Brandt L and Finneran J J 2015 *J. Acoust. Soc. Am.* **138** 2678–91
[56] Medina J M 2011 *Neural Comput.* **23** 1015–46
[57] Moss F, Ward L M and Sannita W G 2004 *Clin. Neurophysiol.* **115** 267–81
[58] Horsthemke W and Lefever R 1984 *Noise-Induced Transitions in Physics, Chemistry, and Biology* (Berlin: Springer) pp 164–200
[59] Lindner B, Garca-Ojalvo J, Neiman A and Schimansky-Geier L 2004 *Phys. Rep.* **392** 321–424
[60] Faisal A A, Selen L P J and Wolpert D M 2008 *Nat. Rev. Neurosci.* **9** 292–303
[61] Harris C M and Wolpert D M 1998 *Nature* **394** 780–4
[62] Stein R B, Gossen E R and Jones K E 2005 *Nat. Rev. Neurosci.* **6** 389–97
[63] Varlet M, Schmidt R C and Richardson M J 2016 *J. Motor Behav.* **48** 122–31
[64] Tolhurst D J, Movshon J A and Dean A F 1983 *Vis. Res.* **23** 775–85
[65] Carandini M 2004 *Plos. Biol.* **2** e264
[66] Moshitch D and Nelken I 2014 *J. Neurosci. Methods* **225** 13–28
[67] Koyama S 2015 *Neural Comput.* **27** 1530–48
[68] Eurich C W and Milton J G 1996 *Phys. Rev.* E **54** 6681–4
[69] Díaz J A, del Barco L J, Jimenez J R and Perez-Ocon F 2001 *Opt. Rev.* **8** 388–96
[70] Díaz J A, del Barco L J, Jimenez J R and Hita E 2001 *Color Res. Appl.* **26** 223–33
[71] Medina J M and Díaz J A 2010 *Ophthal. Physl. Opt.* **30** 511–7
[72] Norwich K H 1977 *Bull. Math. Biol.* **39** 453–61
[73] Coffey W T, Kalmykov Y P and Waldron J T 2004 *The Langevin Equation* (Singapore: World Scientific)
[74] Kesten H 1973 *Acta Math.* **131** 207–48
[75] Redner S 1990 *Am. J. Phys.* **58** 267–73
[76] Sornette D and Cont R 1997 *J. Phys.* I **7** 431–44
[77] Sornette D 1998 *Phys. Rev.* E **57** 4811–3
[78] Takayasu H, Sato A H and Takayasu M 1997 *Phys. Rev. Lett.* **79** 966–9
[79] Nakao H 1998 *Phys. Rev.* E **58** 1591–600
[80] Jaynes E T 1957 *Phys. Rev.* **106** 620–30
[81] Sattin F, Agostini M, Cavazzana R, Serianni G, Scarin P and Vianello N 2009 *Phys. Scr.* **79** 045006
[82] Cramér H 1945 *Mathematical Methods of Statistics* (Princeton, NJ: Princeton University Press)
[83] Vassilev A, Murzac A, Zlatkova M B and Anderson R S 2009 *Vis. Res.* **49** 524–9
[84] Press W, Teukolsky S, Vetterling W and Flannery B 1992 *Numerical Recipes in* C (Cambridge: Cambridge University Press)
[85] Chater N and Brown G D A 1999 *Cognition* **69** B17–24
[86] Naka K I and Rushton W A H 1966 *J. Physiol.* **185** 587–99
[87] Heeger D J 1992 *Vis. Neurosci.* **9** 181–97
[88] Carandini M and Heeger D J 2012 *Nat. Rev. Neurosci.* **13** 51–62
[89] Billock V A and Tsou B H 2005 *J. Opt. Soc. Am.* A **22** 2289–98
[90] Kinouchi O and Copelli M 2006 *Nat. Phys.* **2** 348–52
[91] Albrecht D G and Hamilton D B 1982 *J. Neurophysiol.* **48** 217–37
[92] Sclar G, Maunsell J H R and Lennie P 1990 *Vis. Res.* **30** 1–10
[93] Lennie P and Movshon J A 2005 *J. Opt. Soc. Am.* A **22** 2013–33
[94] Maunsell J H and Gibson J R 1992 *J. Neurophysiol.* **68** 1332–44
[95] Nowak L G, Munk M H J, Girard P and Bullier J 1995 *Vis. Neurosci.* **12** 371–84
[96] Cottaris N P and De Valois R L 1998 *Nature* **395** 896–900
[97] Schmolesky M T *et al* 1998 *J. Neurophysiol.* **79** 3272–8
[98] Solomon S G and Lennie P 2005 *J. Neurosci.* **25** 4779–92
[99] Tailby C, Solomon S G and Lennie P 2008 *J. Neurosci.* **28** 4078–87
[100] Teichner W H and Krebs M J 1972 *Phychol. Rev.* **79** 334–58

J. Stat. Mech. (2016) 093502